Intrinsic Scene Properties from a Single RGB-D Image

Jonathan T. Barron and Jitendra Malik
UC Berkeley
{barron, malik}@eecs.berkeley.edu

Abstract

In this paper we extend the "shape, illumination and reflectance from shading" (SIRFS) model [3, 4], which recovers intrinsic scene properties from a single image. Though SIRFS performs well on images of segmented objects, it performs poorly on images of natural scenes, which contain occlusion and spatially-varying illumination. We therefore present Scene-SIRFS, a generalization of SIRFS in which we have a mixture of shapes and a mixture of illuminations, and those mixture components are embedded in a "soft" segmentation of the input image. We additionally use the noisy depth maps provided by RGB-D sensors (in this case, the Kinect) to improve shape estimation. Our model takes as input a single RGB-D image and produces as output an improved depth map, a set of surface normals, a reflectance image, a shading image, and a spatially varying model of illumination. The output of our model can be used for graphics applications, or for any application involving RGB-D images.

1. Introduction

One of the core problems of computer vision is inferring the properties of a scene (shape, surface normals, illumination, reflectance, etc) that together produced a single observed image. This challenge was first posed as the "intrinsic images" problem [5], but over time this term has come to mean the decomposition of an image into a "shading" image and a "reflectance" image, best exemplified by the Retinex algorithm [15, 18]. Though much progress has been made recently on this subset of the intrinsic images problem [11, 12, 29], the most dramatic progress has come from the SIRFS ("shape, illumination, and reflectance from shading") model [3, 4], which recovers shape and illumination in addition to shading and reflectance, and outperforms standard "intrinsic image" approaches. SIRFS is severely limited by its assumption that input images are segmented images of single objects, illuminated under a single global model of illumination. Natural images, in contrast, contain many shapes which may occlude or support one another, as well as complicated, spatially-varying illumination in the form of shadows, attenuation, and interreflection.

In this paper, we address the problem of inferring a *mixture* of shapes and a *mixture* of illuminations (and implicitly, a shading image and a reflectance image) which explain a natural *scene*. Initially, this problem may seem trivial: why not use segmentation techniques to decompose an image into its constituent objects or illuminations, and then apply SIRFS to each segment? But this is a classic "chicken-or-the-egg" problem, as we cannot reliably segment an image into its constituent shapes and illuminations without first inferring shape and illumination, and vice versa. Additionally, regions of a scene viewed in isolation are often ambiguous, which suggests that information must be shared between regions. We must therefore unify the problems of reconstruction (inferring intrinsic scene properties) and reorganization (grouping an image into meaningful regions), by jointly optimizing over a mixture of shapes, a mixture of illuminations, and the corresponding embedding of each mixture component in the image.

For our technique to work, our shape and light mixtures must respect the structure of the image. We therefore embed our mixtures in the normalized Laplacian of the image, building on normalized cuts [27], as well as Laplacian embeddings [6] and spectral graph theory [8]. This is motivated by the observation that variation in shape and illumination tends to produce gradients and contours in the image, and so our mixtures of shapes and illuminations should be embedded in a space that respects such image variation.

Using shading cues to infer shape, as we are attempting, is understood to work poorly for recovering low-frequency (coarse) shape information [2, 7]. Thankfully, depth data from sensors such as the Kinect [10] is becoming increasing commonplace, and is complementary to shading: binocular disparity (the principle by which the Kinect computes depth) is accurate at coarse scales and inaccurate at fine scales. We will therefore assume the input to our model is an RGB-D image, where "D" is the depth map produced by a sensor such as the Kinect. This makes our problem easier, but in no way trivial — depth maps from sensors such as the Kinect are noisy and incomplete for many rea-

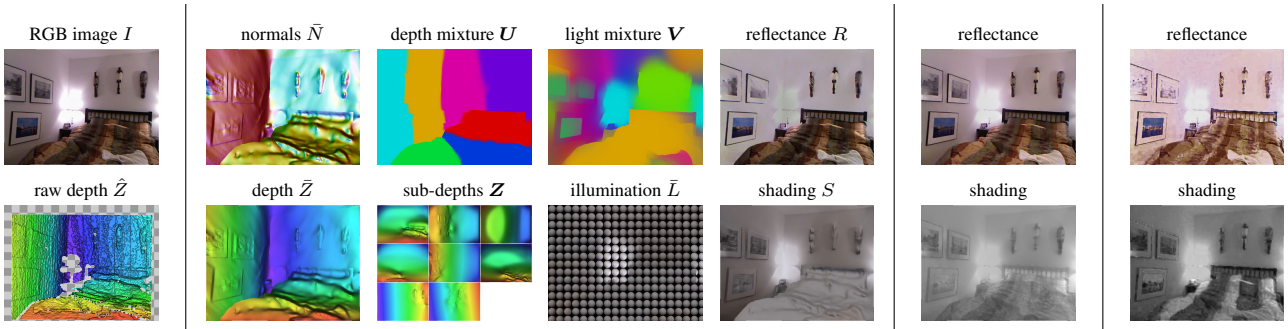

(a) Input (b) Scene-SIRFS (c) Retinex [12, 15] (d) Gehler *et al*. [11]

Figure 1. In 1(a) we have the input to our model: an RGB image and a Kinect depth map from the NYU Depth Dataset [28]. In 1(b) we have the output of our model. Depth maps are visualized with hue corresponding to depth and luminance corresponding to slant, and surface normals are visualized with hue corresponding to orientation, and saturation and luminance corresponding to slant. Mixtures are visualized with hue corresponding to component in the mixture, and intensity corresponding to the probability assigned to that component. Illumination is visualized by rendering a coarse grid of spheres under the spatially-varying illumination. In 1(c) and 1(d) we show the reflectance and shading images produced by two intrinsic image techniques, where 1(d) is the state-of-the-art. See the supplementary material for dozens of additional examples.

sons: occlusion of the structured light, dark objects, sensor noise, alignment errors, quantization, and the inherent physical limitations of binocular disparity. Attempts to use raw depth maps from the Kinect for photometric applications therefore often fail badly. See Figures 1, 5, 6, and 7 for demonstrations of how noisy these depth maps are compared to the depth maps that our model produces.

In Figure 1 we show the output of our model on an RGB-D image from the NYU Depth Dataset [28]. Our model's depth map is a clear improvement over the raw sensor depth map (missing regions have been filled in, noise has been removed, detail has been added), our output shading and reflectance images look better than those of the best "intrinsic image" algorithms, our shape mixture has separated the bed in the foreground from the walls in the background, and our recovered mixture of illuminations captures the complicated illumination in the scene produced by the lamp. Even "mistakes" produced by our model are compelling: our model has attempted to reconstruct the shape of the contents of the photos on the wall, and has modeled these contents with a different illumination environment than the rest of the scene, similarly to how a human might perceive an image within an image. See the supplementary material for dozens of additional examples of our output.

Some past work has addressed similar problems to our own. Forsyth [9] used a spatially-varying model of illumination to address complicated illumination and interreflection, but did not address reflectance or scene-like shape occlusion. Yu *et al*. [30] and Karsch *et al*. [16] have attempted to recover the reflectance and illumination of a scene, but assume known geometry and multiple images, or a user annotation of geometry and illumination, respectively. Hoeim *et al*. [13] and Saxena *et al*. [26] present algorithms for determining the "spatial layout" of a scene, but these shape estimates are coarse, and these models do not recover illumination, reflectance, or shading. Lee *et al*. [19] produces shading and reflectance images given RGB-D data, but requires a video and a fused depth map, and does not produce an illumination model or a refined shape.

Our paper is as follows: in Section 2 we review SIRFS, in Section 3 we introduce Scene-SIRFS, and in Section 4 we introduce the embedding used by our shape and illumination mixtures. In Sections 5 and 6 we present our priors on shape and illumination (our shape prior incorporates the input depth map from the Kinect), and in Section 7 we show how we optimize the resulting inference problem. In Sections 8 and 9 we present experiments on pseudo-synthetic and real RGB-D data, and in Section 10 we conclude.

2. SIRFS

Our model builds upon the "shape, illumination, and reflectance from shading" (SIRFS) model [3, 4], which is a framework for recovering intrinsic scene properties from a single image of a segmented object. SIRFS can be thought of as an extension of classic shape-from-shading models [14] in which reflectance and illumination are recovered in addition to shape. Formally, the SIRFS problem formulation is:

$$\begin{aligned} \underset{R,Z,L}{\text{minimize}} \quad & g(R) + f(Z) + h(L) \\ \text{subject to} \quad & I = R + S(Z, L) \end{aligned} \tag{1}$$

Where R is a log-reflectance image, Z is a depth-map, L is a spherical-harmonic model of illumination [25], and $S(Z, L)$ is a "rendering engine" which produces a log-shading image given Z and L. Z and R are "images" with the same dimensions as I, and L is a 27-dimensional vector. $g(R)$, $f(Z)$, and $h(L)$ are cost functions for reflectance,

shape, and illumination respectively, and can be viewed (roughly) as negative log-likelihoods. We constrain the rendering of our scene properties $R+S(Z,L)$ to be equal to the observed log-intensity image I. Solving this problem corresponds to searching for the least costly (or most likely) explanation $\{Z,R,L\}$ for image I.

Though this model outperforms other intrinsic image techniques, it is critically limited by the requirement that the image contain a single, segmented object. This limitation is due to several factors: 1) SIRFS considers shapes to be composed of a single smooth depth-map Z, and therefore cannot model depth discontinuities, occlusion, etc. 2) SIRFS has a single global model of illumination L, but natural scenes contain spatially-varying illumination due to attenuation, interreflection, cast and attached shadows, etc. 3) SIRFS uses the occluding contour of the object [17], information which is not explicit in natural scenes.

To address these shortcomings, we will use a mixture of shapes and illuminations embedded in a soft segmentation of the scene, and we will use a Kinect depth-map as a surrogate for the information provided by the missing contour cue and to address the inherent limitation of shading for low-frequency shape reconstruction [2, 7]. We call our resulting technique "Scene-SIRFS", as it extends SIRFS from objects to scenes.

3. Scene-SIRFS

The problem formulation of Scene-SIRFS is:

$$\begin{aligned} \underset{R,\boldsymbol{Z},\boldsymbol{\psi},\boldsymbol{L},\boldsymbol{\omega}}{\text{minimize}} \quad & g(R)+\sum_{n=1}^{|\boldsymbol{Z}|} f'(Z^n,U^n)+h'\left(\sum_{m=1}^{|\boldsymbol{L}|} V^m L^m\right) \\ \text{subject to} \quad & I = R+S'(\boldsymbol{Z},\boldsymbol{U},\boldsymbol{L},\boldsymbol{V}) \end{aligned}$$

$$\begin{aligned} U^n &= \frac{\exp(B\psi^n)}{\sum_{n'}\exp(B\psi^{n'})},\ \forall_n \\ V^m &= \frac{\exp(B\omega^m)}{\sum_{m'}\exp(B\omega^{m'})},\ \forall_m \end{aligned} \tag{2}$$

Where $\boldsymbol{Z}=\{Z^n\}$, $\boldsymbol{U}=\{U^n\}$, $\boldsymbol{L}=\{L^m\}$, and $\boldsymbol{V}=\{V^m\}$. This is similar to Equation 1, except that we have sets of shapes and lights instead of a single shape and light, and we have introduced $\boldsymbol{U}$ and $\boldsymbol{V}$, two sets of "images" that define distributions over shapes and lights, respectively. We can think of $\boldsymbol{U}$ as a "visibility" map or a soft relaxation of a $2.5D$ shape representation: if $U^n_{i,j}=1$, then $Z^n_{i,j}$ is visible at pixel (i,j). Similarly, $\boldsymbol{V}$ is the "ownership" of each illumination in $\boldsymbol{L}$, such that if $V^m_{i,j}=1$ then pixel (i,j) is entirely illuminated by L^m. Our prior on shape is now a sum of priors over individual depth maps, where each Z^n in $\boldsymbol{Z}$ is regularized independently (see Section 5). In contrast, our prior on illumination is over the expected illumination of the entire scene, the per-pixel weighted combination of each illumination (see Section 6). Our shape and light mixture probabilities $\boldsymbol{U}$ and $\boldsymbol{V}$ are "images" (where each image corresponds to one mixture component) parametrized by the matrices $\boldsymbol{\psi}$ and $\boldsymbol{\omega}$, respectively, where each column (ψ^n or ω^m) is a 17-dimensional vector parametrizing the "ownership" of that shape or light mixture in the scene. The probabilities $\boldsymbol{U}$ and $\boldsymbol{V}$ are the product of each weight matrix with B (the eigenvectors of the normalized Laplacian of the RGB image, explained in later) passed through a softmax function[1]. We use 8 shapes and illuminations in our mixtures for all experiments ($|\boldsymbol{L}|=|\boldsymbol{Z}|=8$) though this is arbitrary. See Figure 1 for a visualization of these mixtures.

For the purpose of optimization, we need to define the normal field of this mixture of shapes $N'(\boldsymbol{Z},\boldsymbol{U})$. We cannot use the surface normals of the expected depth map $N(\sum Z^n U^n)$ as this cannot model depth-discontinuities. We also cannot use the expected surface normals of the mixture of shapes $\sum U^n N(Z^n)$ as this normal field may have vectors of non-unit length. We will therefore linearize each Z^n into a set of partial derivatives in x and y, take the expectation of those with respect to $\boldsymbol{U}$, and then construct a normal field from those expected partial derivatives. This gives us a proper normal field where each Z^n's influence at pixel (i,j) is proportional to $U^n_{i,j}$. Formally:

$$\begin{aligned} N'(\boldsymbol{Z},\boldsymbol{U}) &= \left\{\frac{D^x}{D^m},\frac{D^y}{D^m},\frac{1}{D^m}\right\} \\ D^x=\sum_{n=1}^{|\boldsymbol{Z}|}U^n(Z^n*h^x),\quad & D^y=\sum_{n=1}^{|\boldsymbol{Z}|}U^n(Z^n*h^y) \\ D^m &= \sqrt{1+(D^x)^2+(D^y)^2} \\ h^x=\frac{1}{8}\begin{bmatrix}1&0&-1\\2&0&-2\\1&0&-1\end{bmatrix},\quad & h^y=\frac{1}{8}\begin{bmatrix}1&2&1\\0&0&0\\-1&-2&-1\end{bmatrix} \end{aligned} \tag{3}$$

Let $S'(\cdot)$ be our rendering engine for our mixtures, which computes the normal field of the mixture of shapes and renders it such that the spherical harmonic illumination at pixel (i,j) is a linear combination of all L^m, weighted by $V^m_{i,j}$:

$$S'(\boldsymbol{Z},\boldsymbol{U},\boldsymbol{L},\boldsymbol{V}) = S\left(N'(\boldsymbol{Z},\boldsymbol{U}),\sum_{m=1}^{|\boldsymbol{L}|}V^m L^m\right) \tag{4}$$

Where $S(\cdot)$ is the rendering engine in standard SIRFS [3].

Though the spatially varying illumination parametrized by $\{\boldsymbol{L},\boldsymbol{V}\}$ is capable of explaining away shadows, specularities, and interreflections, no attempt has been made to ensure that the illumination is globally consistent. Though this may seem unsettling, the human visual system has similar properties: people tend not to notice inconsistent shadows or impossible illumination [24].

[1] in a slight abuse of notation, $\boldsymbol{U}$ and $\boldsymbol{V}$ are simultaneously treated as sets of images and as matrices whose columns are vectorized images.

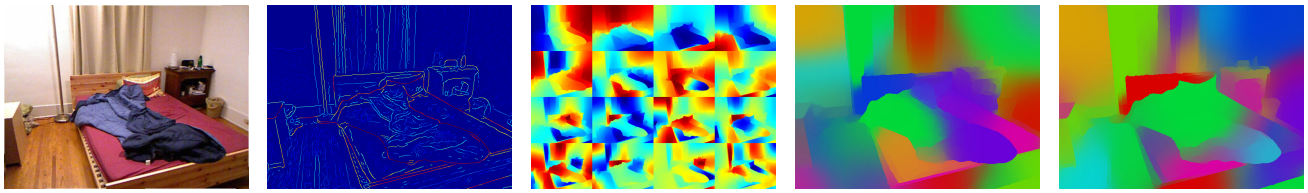

(a) Input Image (b) Multiscale Pb (c) Eigenvector basis (d) A random mixture (e) Another random mixture

Figure 2. A visualization of the embedding used in our shape and light mixtures. In 2(a), we have an input image. In 2(b) we have the output of multiscale Pb on the input image, and in 2(c) we have the 16 smallest eigenvectors (ignoring the eigenvector that is all 1's) of mPb using the intervening contour cue [1]. Each shape's and light's "ownership" of the image is parametrized by a 17-dimensional vector, which is projected onto the eigenvector basis and passed through a softmax function to yield the probability of each pixel belonging to each mixture component. 2(d) and 2(e) are visualizations of two random mixtures with 8 components (such as $\boldsymbol{U}$ or $\boldsymbol{V}$) where the weight vectors ($\boldsymbol{\psi}$ or $\boldsymbol{\omega}$) are generated randomly (sampled from a Gaussian).

4. Mixture Embedding

Using a mixture of shapes and illuminations is necessary to model depth discontinuities and spatially varying illumination, both of which tend to produce variation in the image in the form of contours, intensity variation, texture gradients, etc. It therefore follows that we should embed the shape and light mixtures in some space where the "ownership" of each mixture adheres to the segmentation of the scene. This simplifies inference, as we restrict our attention to only mixtures of the shapes and lights that are supported by evidence in the image. This is similar to the motivation for the use of superpixels as a substrate for inference in CRF-type models, though our experience suggests that superpixels are a poor embedding for this task, as they are too "hard". We will instead embed each mixture component in a more "soft" embedding: the eigenvectors of the normalized Laplacian of a graph corresponding to the input RGB image [27]. We construct our embedding as follows: given an image, first we compute the multiscale Pb of that image [1, 22]. We then form an affinity matrix from mPb using the intervening contour cue [20], and compute the 17 eigenvectors $\{\mathbf{u}_i\}$ corresponding to the smallest eigenvalues (the first eigenvector is all 1's). For eigenvectors 2 through 17, we subtract the mean from each $\mathbf{u}_i$ and divide each by its standard deviation, and then concatenate these normalized eigenvectors into a matrix B, with one column per-pixel. B is our embedding space, in that each mixture component is defined by a 17-dimensional vector, whose inner product with B defines how dominant that mixture component is at every pixel in the input image. A similar embedding is used in [23], for the purpose of combining recognition and segmentation. See Figure 2 for a visualization of this embedding.

It may seem unusual that we construct our embedding using only RGB information, instead of using the complete RGB-D image. We do this because the depth images are often mis-aligned and noisy enough that it is challenging to construct a single accurate contour signal from both sources of information. Using only the image to create an embedding circumvents the noise in the depth map and forces the reconstructed shape to be aligned with the image.

Our prior on reflectance $g(\cdot)$ is exactly the same as in [3]. In Sections 5 and 6 we will define $f'(\cdot)$ and $h'(\cdot)$, our priors on our shape and illumination mixtures, respectively.

5. Shape Priors and Kinect Images

Our prior on shape is a modification of that of [3]. We use a linear combination of the smoothness and flatness terms $f_\kappa(Z)$ and $f_f(Z)$ introduced in [4] and refined in [3], without the occluding contour prior (as we no longer know the occluding contours of objects in the scene) with an additional term $f_{\hat{Z}}(Z, U)$ that incorporates knowledge from the raw sensor depth map produced by the Kinect $\hat{Z}$:

$$f'(Z, U) = \lambda_\kappa f_\kappa(Z) + \lambda_f f_f(Z) + \lambda_{\hat{Z}} f_{\hat{Z}}(Z, U) \qquad (5)$$

Where $f_\kappa(Z)$ minimizes the local variation of mean curvature of Z, encouraging Z to be smooth, and $f_f(Z)$ minimizes the slant of Z, encouraging Z to be fronto-parallel. We introduce $f_{\hat{Z}}(Z, U)$, which encourages Z to be similar to the raw sensor depth map if Z is thought to be "visible" according to U. Crucially, we apply this prior to each individual depth map in our mixture rather than to some average depth map. This encourages the scene's constituent depth maps to be smooth while allowing the expected depth map implied by the mixture to vary abruptly, thereby allowing us to model depth discontinuities and occlusion.

We use version 2 of the NYU Depth Dataset [28], which consists of RGB images and aligned Kinect depth maps. Because Kinect depth maps often have gaps, the dataset also provides inpainted depth maps. We will use the raw depth maps rather than the inpainted ones, as our algorithm will implicitly denoise and inpaint depth during inference. In addition to gaps, Kinect depth maps have different kinds of noise. First: the depth and RGB images are often not well-aligned — not enough to matter for most recognition tasks, but enough to affect photometric or reconstruction

tasks. Second: the disparity recovered by the Kinect is often noisy, presumably due to sensor noise or errors in the Kinect's stereo algorithm. Third: the disparity is quantized, which leads to step-like artifacts in depth.

We must construct a loss function to encourage our recovered depth Z to resemble the raw sensor depth $\hat{Z}$. First, let us approximate the upper bound of the error introduced by quantizing the disparity corresponding to $\hat{Z}$:

$$Z_{i,j}^{err} = (1.4233 \times 10^{-5})\hat{Z}_{i,j}^2 + 2 \quad (6)$$

where $\hat{Z}$ and Z^{err} are in centimeters. The first term is derived from the baseline of the Kinect, and the second term is additional ad-hoc slack. We assume that if the difference between $Z_{i,j}$ and $\hat{Z}_{i,j}$ at pixel (i,j) is less than $Z_{i,j}^{err}$, then that difference is due to quantization and therefore should be ignored. Errors greater than $Z_{i,j}^{err}$ will be robustly penalized, as they probably are due to sensor noise or alignment errors. Our loss function is:

$$f_{\hat{Z}}(Z,U) = \sum_{i,j} U_{i,j} \max\left(0, \left|Z_{i,j} - \hat{Z}_{i,j}\right| - Z_{i,j}^{err}\right)^{\alpha_{\hat{Z}}} \quad (7)$$

Minimizing this is equivalent to assuming noise is uniformly distributed over a region of size $2Z_i^{err}$ and is hyper-Laplacian outside of that range. The loss is proportional to $U_{i,j}$, which means that $Z_{i,j}$ need only resemble $\hat{Z}_{i,j}$ if our model believes that this depth map is in the foreground at pixel (i,j). $\alpha_{\hat{Z}}$ controls the shape of the tail of the distribution, and is tuned with cross-validation on the training set (along with λ_κ, λ_f, and $\lambda_{\hat{Z}}$), which sets $\alpha_{\hat{Z}} = 0.7$.

6. Illumination Priors

Our prior on illumination is a simple extension of the illumination prior of [3] to a mixture model, in which we regularize the expectation of a set of illuminations instead of a single illumination. Given $\boldsymbol{L}$ (our set of spherical harmonic illuminations) and $\boldsymbol{V}$ (our set of "images" that define a per-pixel distribution over our illuminations), we can compute the expectation of this model at each pixel of the image:

$$\bar{L}_{i,j} = \sum_{m=1}^{|\boldsymbol{L}|} V_{i,j}^m L^m \quad (8)$$

Where $\bar{L}_{i,j}$ is a 27-dimensional vector describing the effective illumination at pixel (i,j) in the image. Our prior on illumination is the negative log-likelihood of a multivariate normal distribution, applied to each 27-dimensional "pixel" in $\bar{L}$:

$$h'(\bar{L}) = \lambda_L \sum_{i,j} (\bar{L}_{i,j} - \boldsymbol{\mu}_L)^{\mathrm{T}} \Sigma_L^{-1} (\bar{L}_{i,j} - \boldsymbol{\mu}_L) \quad (9)$$

Where $\boldsymbol{\mu}_L$ and Σ_L are the parameters of the Gaussian we learn on the training set, and λ_L is the multiplier on this prior (learned through cross-validation on the training set).

(a) Kinect Depth Map (b) Mixture of Gaussians (c) Plane-Fit Depth Map

Figure 3. We initialize the depth maps in our shape mixture by fitting a mixture of Gaussians to the (x,y,z) coordinates of depth-map pixels, and then fitting a plane to each Gaussian. 3(a) shows the raw depth map, 3(b) shows the posterior probability of each pixel under each mixture component, and 3(c) shows the fitted planes composed into one depth map according to hard assignments under the mixture of Gaussians.

7. Initialization & Optimization

Optimization of our model is similar to that of [3]. We absorb the $I = R + S(\cdot)$ constraint in Equation 2 by rewriting $g(R)$ as $g(I - S(\cdot))$, thereby eliminating R as a free parameter. In optimization we internally represent each depth map Z^n as a pyramid, and whiten each illumination L^m according to $\{\boldsymbol{\mu}_L, \Sigma_L\}$. We vectorize those our pyramid-depths, whitened illuminations, and mixture weights $\{\boldsymbol{\psi}, \boldsymbol{\omega}\}$ into one state vector, and then minimize the loss in Equation 2 using L-BFGS.

This optimization problem is non-convex, and so it is sensitive to initialization. Because the scenes in the NYU dataset are mostly composed of planar surfaces, we will initialize each depth map Z^i in $\boldsymbol{Z}$ to a plane such that the scene is well-described by the set of planes. To do this, we fit a mixture of Gaussians to the (x,y,z) coordinates of each pixel in $\hat{Z}$ (in image coordinates) using EM with 50 random restarts. Once EM converges we have n multivariate Gaussians, each parametrized by a mean μ and a covariance matrix Σ. If a Gaussian does indeed describe a roughly-planar surface, then Σ will be elongated in two directions, and narrow in the third. This means that the Gaussian is well described by the plane satisfying $v^{\mathrm{T}}([x,y,z] - \mu) = 0$, where v is the eigenvector corresponding to the smallest eigenvalue of Σ. We initialize each surface in our mixture to its corresponding plane in our mixture of Gaussians, by solving for z at every pixel. See Figure 3 for a visualization.

This plane-fitting sometimes produces poor results on our synthetic dataset, because our synthetic scenes contain mostly fronto-parallel objects stacked on top of each other. Therefore, in our synthetic experiments we initialize the depth maps by doing K-means (with 50 random restarts) on just the z values in the scene, and then initializing each depth map to be a centroid, thereby constraining the initial depth-planes to be fronto-parallel.

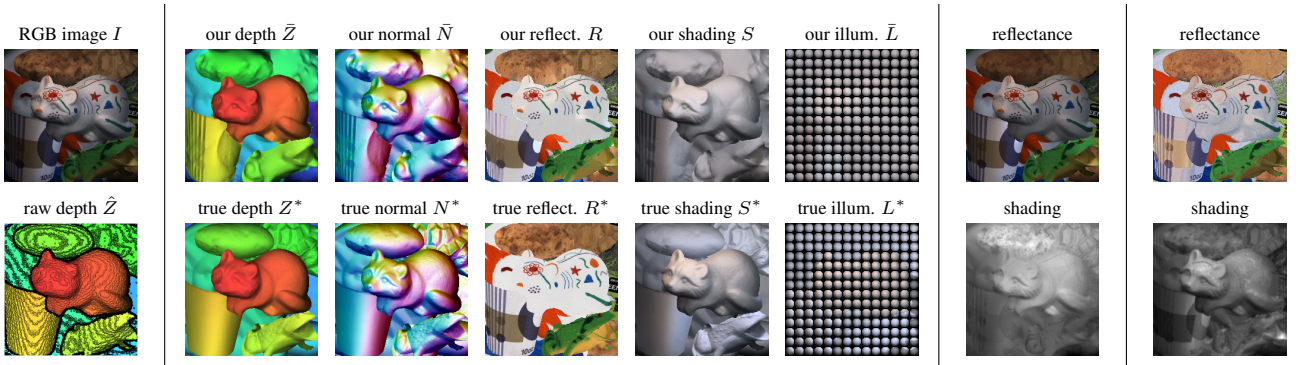

(a) Input (b) Scene-SIRFS / Ground-Truth (c) Retinex [12, 15] (d) Gehler *et al.* [11]

Figure 4. A test-set scene from our pseudo-synthetic scene dataset. In 4(a) we have the input to our model: an RGB image and a noisy Kinect-like depth map. In 4(b) we have the depth map, surface normals, reflectance, shading, and spatially-varying illumination that our model produces, and the corresponding ground-truth scene properties on the bottom. In 4(c) and 4(d) we show the shading and reflectance images produced by the best-performing intrinsic image algorithms. See the supplementary material for additional similar figures.

8. Experiment - Pseudo-synthetic Data

The primary goal of this paper is to produce a model that works well on actual Kinect images. However, it is extremely difficult to produce ground-truth shape, reflectance, shading, and illumination models for real-world natural scenes. Thankfully, using the MIT Intrinsic Images dataset [12] extended with the ground-truth depth maps produced by Berkeley [4] we can compose pseudo-synthetic scenes that emulate natural scenes. In the supplementary material, we explain how we compose these objects into heavily cluttered scenes, which display occlusion and spatially-varying illumination. We also generate noisy Kinect-like depth maps from ground-truth depth maps for use as input to our model. Examples of this data can be seen in Figure 4, and in the supplementary material. We present this dataset not because we believe it to be a perfect surrogate for reality, but because it is the closest approximation to reality for which we have exhaustive ground-truth, allowing us to train our model and tune hyperparameters (on the training set) and compare our model to others (on the test set).

Algorithm	Z-MAE	N-MAE	s-MSE	r-MSE	rs-MSE	L-MSE	Avg.
(1) Color Retinex [12, 15]	-	-	0.0230	0.0364	0.0354	-	-
(2) Tappen *et al.* 2005 [29]	-	-	0.0281	0.0337	0.0387	-	-
(3) Gehler *et al.* 2011 [11]	-	-	0.0181	0.0224	**0.0216**	-	-
(4) Kinect Only	**5.09**	0.5799	-	-	-	-	-
(5) SIRFS [3]	114.82	0.6841	0.0181	0.0202	0.0289	0.0241	0.1647
(6) SIRFS + Segmentation	57.43	0.7600	0.0176	0.0200	0.0296	0.0210	0.1458
(A) **Scene-SIRFS (Complete)**	10.91	**0.2618**	**0.0101**	**0.0184**	0.0227	**0.0166**	**0.0764**
(B) Scene-SIRFS ($\lambda_{\bar{Z}} = 0$)	122.67	0.6454	0.0134	0.0203	0.0256	0.0199	0.1491
(C) Scene-SIRFS (No Initialization)	11.06	0.3000	0.0113	0.0233	0.0263	0.0176	0.0860
(D) Scene-SIRFS ($\|\boldsymbol{Z}\| = 1$)	22.72	0.5123	0.0179	0.0284	0.0348	0.0237	0.1302
(E) Scene-SIRFS ($\|\boldsymbol{L}\| = 1$)	11.64	0.2754	0.0163	0.0313	0.0269	0.0211	0.0988
(F) Scene-SIRFS ($\|\boldsymbol{Z}\| = \|\boldsymbol{L}\| = 1$)	24.59	0.5285	0.0292	0.0587	0.0523	0.0213	0.1708
(G) Scene-SIRFS (Z only)	9.82	0.2877	-	-	-	-	-
(H) Scene-SIRFS (Z only, $\|\boldsymbol{Z}\| = 1$)	24.69	0.5552	-	-	-	-	-

Table 1. Our results on the test set of our pseudo-synthetic dataset. Shown are the geometric means of six error metrics (detailed in the supplementary material) across the test set, and an "average" error (the geometric mean of the other error metrics). Z-MAE measures shape errors, N-MAE measures surface-normal errors, s-MSE, r-MSE, and rs-MSE measure shading and reflectance errors, and L-MSE measures illumination errors. If an algorithm does not produce a certain scene property, its error is left blank. (1)-(3) are intrinsic image algorithms, which produce shading and reflectance images from an RGB image, where (3) is the current state-of-the-art. (4) evaluates the error of the noisy Kinect-like depth maps we use as input. (5) is the SIRFS model that we build upon, and is equivalent to our model without any mixture models or a Kinect depth map. (6) is SIRFS run in isolation on the segments produced by normalized cuts. In addition to our complete model (A), we present several ablations. (B) has no Kinect information, (C) has no initialization, and (D)-(F) omit one or both of the shape or light mixtures. (G) is a shape-denoising algorithms in which we omit the RGB image and just optimize over shape with respect to our prior on shapes, and (H) is (G) with a single depth map, instead of a mixture model.

Table 1 compares our model's performance to other intrinsic images techniques and to ablations of our model. The shading and reflectance images produced by our model beat or match the best intrinsic image algorithms. The surface normals produced by our model have half of the error of the input, though for absolute depth error we do not improve. This is consistent with the limits of shading, as shading directly informs the surface normal, but only implicitly informs absolute depth. Our performance is similar to that of SIRFS in terms of reflectance, but much better in all other respects. A naive extension of SIRFS to scenes (in which we use normalized cuts to segment each image into 16 segments and run SIRFS on each segment in isolation) performs similarly to basic SIRFS. The source of our advantage over SIRFS is shown through our ablations — removing either the shape or the illumination mixture components hurts performance on every error metric, and removing the Kinect depth map hurts performance on the depth and normal error metrics, though not the shading or reflectance metrics. The degenerate case of our model which only denoises the depth map and ignores the RGB image performs surprisingly well

in terms of error relative to the ground-truth shape and normal field. However, we believe this mostly reflects a bias in our error metrics towards overly smooth shapes, which the shape-denoising ablation produces (see Figure 7).

9. Experiment - Kinect Data

To qualitatively evaluate our model, we sampled several images from version 2 of the NYU Depth Dataset [28], and ran them through our model (all using the same hyperparameter setting as in our pseudo-synthetic experiment). The output of our model can be seen in Figure 1 and in the supplementary material. We compare against two intrinsic image algorithms: Retinex [12, 15] and Gehler *et al*. [11].

Our shading and reflectance images generally look much better than those produced by the intrinsic image algorithms, and our recovered depth and surface normals look much better than the input Kinect image. Our spatially varying illumination captures shadowing and interreflections, and looks reasonable. The primary cause of errors in our model appears to be over-smoothing of the depth map, which we believe is because the error metrics with which we cross-validate our model tend to favor conservative parameter settings, and because MAP estimation for tasks such as ours tends to produce overly conservative output [21].

One way to evaluate the accuracy of our model is to use it in graphics applications. In Figures 5 and 6 we use our output to re-render the input image under different camera viewpoints and under different illumination conditions. Our renderings look significantly better than renderings produced with the inpainted Kinect depth map provided by the NYU dataset. Changing the viewpoint with the raw Kinect depths creates jagged artifacts at the edges of shapes, while our depth (which is both denoised and better-aligned to the image) looks smooth and natural at object boundaries. Relighting the raw Kinect depth produces terrible artifacts, as the surface normals of the raw depth are very inaccurate due to noise and quantization, while relighting our output looks reasonable, as the surface normals are cleaner and reflectance has been separated from shading. In Figure 7 we see that the depth maps our model produces are less noisy than the NYU depth maps, and more detailed than the output of the shape-denoising ablation of our model, demonstrating the importance of the complete model.

10. Conclusion

We have presented Scene-SIRFS, a variant of SIRFS that takes as input images of natural scenes rather than images of segmented objects. We have done this by generalizing SIRFS into a mixture model of shapes and illuminations, and by embedding those mixtures into a soft segmentation of an image. We additionally use the noisy depth maps in RGB-D data to improve low-frequency shape estimation.

The output of our model can be used for graphics applications such relighting or re-orienting the camera, and it is easy to imagine other applications such as inserting objects, modifying reflectances, or white balancing. Our model improves the initial depth map by removing noise, adding fine-scale shape detail, and aligning the depth to the RGB image, all of which presumably would be useful in any application involving RGB-D images. Perhaps most importantly, our model takes an important step towards solving one of the grand challenges in vision — inferring all intrinsic scene properties from a single image.

Acknowledgements: J.B. was supported by NSF GRFP and ONR MURI N00014-10-10933.

References

[1] P. Arbelaez, M. Maire, C. Fowlkes, and J. Malik. Contour detection and hierarchical image segmentation. *TPAMI*, 2011.

[2] J. T. Barron and J. Malik. High-frequency shape and albedo from shading using natural image statistics. *CVPR*, 2011.

[3] J. T. Barron and J. Malik. Color constancy, intrinsic images, and shape estimation. *ECCV*, 2012.

[4] J. T. Barron and J. Malik. Shape, albedo, and illumination from a single image of an unknown object. *CVPR*, 2012.

[5] H. Barrow and J. Tenenbaum. Recovering intrinsic scene characteristics from images. *Computer Vision Systems*, 1978.

[6] M. Belkin and P. Niyogi. Laplacian eigenmaps for dimensionality reduction and data representation. *Neural Computation*, 2002.

[7] A. Blake, A. Zisserman, and G. Knowles. Surface descriptions from stereo and shading. *IVC*, 1986.

[8] F. R. K. Chung. *Spectral Graph Theory*. American Mathematical Society, 1997.

[9] D. A. Forsyth. Variable-source shading analysis. *IJCV*, 2011.

[10] B. Freedman, A. Shpunt, M. Machline, and Y. Arieli. Depth mapping using projected patterns. *US Patent*, 2009.

[11] P. Gehler, C. Rother, M. Kiefel, L. Zhang, and B. Schoelkopf. Recovering intrinsic images with a global sparsity prior on reflectance. *NIPS*, 2011.

[12] R. Grosse, M. K. Johnson, E. H. Adelson, and W. T. Freeman. Ground-truth dataset and baseline evaluations for intrinsic image algorithms. *ICCV*, 2009.

[13] D. Hoiem, A. A. Efros, and M. Hebert. Recovering surface layout from an image. *IJCV*, 2007.

[14] B. K. P. Horn. Shape from shading: A method for obtaining the shape of a smooth opaque object from one view. Technical report, MIT, 1970.

[15] B. K. P. Horn. Determining lightness from an image. *Computer Graphics and Image Processing*, 1974.

[16] K. Karsch, V. Hedau, D. Forsyth, and D. Hoiem. Rendering synthetic objects into legacy photographs. *SIGGRAPH Asia*, 2011.

[17] J. Koenderink. What does the occluding contour tell us about solid shape? *Perception*, 1984.

[18] E. H. Land and J. J. McCann. Lightness and retinex theory. *JOSA*, 1971.

Figure 5. After a model is recovered, the camera can be moved and the input image (left) can be shown from a different viewpoint (right). Such a warping could be produced using just the smoothed Kinect depth maps provided in the NYU dataset (middle), but these images have jagged artifacts at surface and normal discontinuities. Both renderings, of course, contain artifacts in occluded regions.

Figure 6. After a model is recovered, the spherical harmonic illuminations can be replaced (here we use randomly generated illuminations) and the input image (left) can shown under a different illumination (right). The middle image is our attempt to produce similar re-lit images using only the inpainted depth maps in the NYU dataset, which look noticeably worse due to noise in the depth image and the fact that illumination and reflectance have not been decomposed.

[19] K. J. Lee, Q. Zhao, X. Tong, M. Gong, S. Izadi, S. U. Lee, P. Tan, and S. Lin. Estimation of intrinsic image sequences from image+depth video. *ECCV*, 2012.

[20] T. K. Leung and J. Malik. Contour continuity in region based image segmentation. *ECCV*, 1998.

[21] A. Levin, Y. Weiss, F. Durand, and W. Freeman. Understanding and evaluating blind deconvolution algorithms. *CVPR*, 2009.

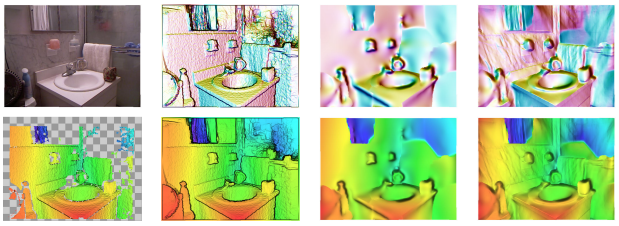

(a) input (b) NYU depth (c) denoised depth (d) our depth

Figure 7. One output of our model is a denoised depth-map. In 7(a) we have the RGB-D input to our model, demonstrating how noisy and incomplete the raw Kinect depth map can be. 7(b) shows the inpainted normals and depth included in the NYU dataset [28], where holes have been inpainted but there is still a great deal of noise, and many fine-scale shape details are missing. 7(c) is from an ablation of our model in which we just denoise/inpaint the raw depth map ("model H" in our ablation study), and 7(d) is from our complete model. The NYU depth map is noisy at high frequencies and does not model depth discontinuities (hence the dark "slant" lines outlining each object), and our "denoising" model tends to oversmooth the scene, but our complete model has little noise while recovering much of the detail of the scene and correctly separating objects into different layers.

[22] M. Maire, P. Arbelaez, C. C. Fowlkes, and J. Malik. Using contours to detect and localize junctions in natural images. *CVPR*, 2008.

[23] S. Maji, N. Vishnoi, and J. Malik. Biased normalized cuts. *CVPR*, 2011.

[24] Y. Ostrovsky, P. Cavanagh, and P. Sinha. Perceiving illumination inconsistencies in scenes. *Perception*, 2005.

[25] R. Ramamoorthi and P. Hanrahan. An Efficient Representation for Irradiance Environment Maps. *CGIT*, 2001.

[26] A. Saxena, M. Sun, and A. Ng. Make3d: learning 3d scene structure from a single still image. *TPAMI*, 2008.

[27] J. Shi and J. Malik. Normalized cuts and image segmentation. *TPAMI*, 2000.

[28] N. Silberman, D. Hoiem, P. Kohli, and R. Fergus. Indoor segmentation and support inference from rgbd images. *ECCV*, 2012.

[29] M. F. Tappen, W. T. Freeman, and E. H. Adelson. Recovering intrinsic images from a single image. *TPAMI*, 2005.

[30] Y. Yu, P. Debevec, J. Malik, and T. Hawkins. Inverse global illumination: recovering reflectance models of real scenes from photographs. *SIGGRAPH*, 1999.